Molecular dynamics simulations of spontaneous spreading of a nanodroplet on solid surfaces

2011 Fluid Dyn. Res. 43 015507

(http://iopscience.iop.org/1873-7005/43/1/015507)

IOP PUBLISHING FLUID DYNAMICS RESEARCH

Fluid Dyn. Res. **43** (2011) 015507 (22pp) doi:10.1088/0169-5983/43/1/015507

Molecular dynamics simulations of spontaneous spreading of a nanodroplet on solid surfaces

Nahid Sedighi[1], **Sohail Murad**[1,2] **and Suresh K Aggarwal**[1]

[1] Department of Mechanical and Industrial Engineering, University of Illinois at Chicago, Chicago, IL, USA
[2] Department of Chemical Engineering, University of Illinois at Chicago, Chicago, IL, USA

E-mail: ska@uic.edu

Received 6 August 2010, in final form 26 October 2010
Published 13 December 2010
Online at stacks.iop.org/FDR/43/015507

Communicated by A D Gilbert

Abstract

The dynamics of spontaneous spreading of nano-sized droplets on solid surfaces were investigated using molecular dynamics simulations. The spreading behavior was analyzed in terms of the temporal evolution of instantaneous spreading diameter and contact angle for surfaces with different wetting characteristics. The computational model was validated through qualitative comparison with existing numerical and experimental data, including correlations for the variation of dynamic contact angle and spreading diameter. The results indicated that the spreading dynamics are mainly governed by surface and viscous forces. The spontaneous spreading process on a wettable surface can be described by three different stages, namely the initial, intermediate and final stages. The initial stage is characterized by the development of a precursor film, which moves ahead of the droplet, whereas the intermediate and final spreading stages are governed by a balance between surface and viscous forces. Simulations were used to develop correlations for the temporal variation of contact angle and spreading diameter for wettable, partially wettable and non-wettable surfaces. These correlations were found to be closer to those based on the molecular kinetic model than to those based on the hydrodynamic model. The results were further analyzed to obtain correlations for the effect of droplet size on the spreading parameters. These correlations indicated that the normalized spreading diameter and contact angle scale with non-dimensional drop diameter as $D_m/D_0 \propto D_0^{-0.6\pm0.04}$ and $\theta_R \propto D_0^{0.67\pm0.12}$ and the normalized spreading time scales as $t \propto D_0^{0.25\pm0.05}$. Global surface energy and viscous dissipation energy considerations were used to provide a physical basis for these correlations. Significant differences were observed between the dynamics of spontaneous and forced spreading, especially with respect to the effect of droplet size on the spreading behavior.

(Some figures in this article are in colour only in the electronic version)

0169-5983/11/015507+22$33.00

1. Introduction

The spreading of a droplet on solid surfaces is important for a wide range of applications, including propulsion, surface coating, spray painting, spray cooling, ink-jet printing, agricultural sprays and biological sensors. In coating applications, a spatially uniform coating requires fundamental understanding of the spreading dynamics, characterized by the dynamic contact angle and spreading diameter. In many propulsion applications, the wall impingement of liquid droplets often determines the fuel vapor distribution and thereby the combustion and emission characteristics. In spray cooling, the droplet spreading has a strong influence on the heat transfer characteristics. In numerous applications involving nanodevices, such as nanofluidics and microelectronics, droplet spreading represents a fundamental process. For instance, ink-jet printing, which involves droplet deposition and spreading on a moving or stationary surface, is a key technology in microelectronics and the fabrication of micro- and nanodevices. In microelectronics, metallic conducting tracks are produced by depositing a series of droplets, containing an organometallic compound (or metal nanoparticles) dissolved in a carrier fluid, on a moving substrate (Lee and Kim 2000). Understanding the fundamental spreading processes is important for controlling the quality, width and morphological properties of the track formed.

Characterizing the dynamic spreading behavior has been extremely challenging due to the multitude of scales, ranging from continuum to molecular, and a wide variety of applications involving different fluids and substrates. In a previous study (Sedighi *et al* 2010), we employed molecular dynamics (MD) simulations to examine the spreading behavior of nano-sized droplets impacting (we refer to this as forced spreading because of the considerable impact with which the droplet makes contact with the surface) orthogonally on surfaces with different wettability characteristics. The correlations were developed to characterize the dependence of dynamic spreading diameter and contact angle on the droplet size. In the present study, we employ a similar MD methodology to investigate the spontaneous spreading behavior of nano-sized droplets placed on horizontal surfaces. Since many applications involve droplet spreading with negligible inertial effects, it is of interest to examine how the spreading dynamics and scaling relationships are modified in the absence of inertial forces. Moreover, as discussed below, several previous studies have focused on this regime and provided scaling laws for the spreading diameter and contact angle.

When a droplet is placed on a solid surface with negligible impact velocity, it spreads spontaneously on the surface under the influence of capillary and viscous forces (Semal *et al* 1999). The spreading process is initially characterized by the motion of a precursor film and subsequently by the dynamics of a contact line (Decamps and De Coninck 2000). Previous studies have employed mainly two approaches, based on the hydrodynamic model (Shikhmurzaev 1977, Cox 1986) and the molecular kinetic model (Blake and Haynes 1969, Cherry and Holmes 1969), to describe this spreading process. In the first approach, droplet spreading is described from a continuum viewpoint by considering the balance between capillary and viscous forces (Voinov 1976, Shikhmurzaev 1977, Cox 1986), and scaling laws have been developed for the temporal evolution of the spreading radius and contact angle (De Coninck *et al* 2001) in the form $R(t) \sim t^{1/10}$ and $\theta(t) \sim t^{-3/10}$. The second approach is based on the molecular kinetic theory (Glasstone *et al* 1941, Blake and Haynes 1969) and describes droplet spreading in terms of the microscopic frequency (k) and displacement (λ) of the movement of individual molecules and atoms in the vicinity of the contact line (Blake 1968, 1993, Ruckenstein and Dunn 1977). Here, the variation of the spreading radius and contact angle with time is given as (Tanner 1979) $R(t) \sim t^{1/7}$ and $\theta(t) \sim t^{-3/7}$. Experimental studies have also been reported for validating these models (Lopez *et al* 1976,

Marmur 1983). Another important process in spontaneous spreading is the development of a precursor film in front of the droplet. For a wettable surface, it has been shown that a precursor film consisting of one or more monomolecular layers spreads in front of the macroscopic part of the droplet, and its spread radius varies as $R(t) \propto \sqrt{t}$ (de Gennes 1985).

While the above-described features of spontaneous spreading are relatively well understood for macroscopic droplets (Leger and Joanny 1992), they have not been fully investigated for nanodroplets. The experimental observations for macroscopic droplets may not be easily interpreted for nanoscale droplets, due to the small scales involved. In addition to impurities, surface heterogeneities and pinning of contact angle can influence the droplet behavior at the nanoscale. Moreover, most previous numerical studies have considered sessile droplets with two-dimensional and cylindrical configurations (Heslot *et al* 1989, Yang 1991, De Coninck *et al* 1995, de Ruijter *et al* 1999a, 1999b, Kandlikar *et al* 2001, He and Hadjiconstantinou 2003). Many of these studies have focused on the spreading of a precursor film (Heslot *et al* 1989, De Coninck *et al* 1995). De Coninck *et al* (1995) examined the spreading dynamics of liquid drop on a solid substrate, and observed that the spreading rate of the precursor film follows $R(t) \propto t^{0.46\pm0.03}$. Heine *et al* (2003) numerically examined the dynamics of a precursor film and the bulk droplet using large hemispherical drops, and observed the $\sqrt{t}$ behavior for the precursor foot in agreement with the molecular kinetic model. In a subsequent study (Heine *et al* 2004), they examined the spreading dynamics of nanodroplets in a cylindrical geometry and noted that the scaling laws are modified in this geometry. For instance, they reported that in cylindrical geometry, the scaling law for the spreading radius, based on the molecular kinetic theory, becomes $r(t) \sim t^{1/5}$ compared to $r(t) \sim t^{1/7}$ for spherical droplets.

He and Hadjiconstantinou (2003) performed simulations of droplets spreading on a surface, and showed that Tanner's law could be recovered even if van der Waals effects and the resulting precursor film were limited to distances of the order of three atomic diameters from the substrate. They suggested that the precursor theory of de Gennes (1985) could be generalized to precursors of molecular thickness in which flow is not characterized by the continuum model. Yang *et al* (1991) studied the spreading of liquid drops on solid surfaces by considering a liquid–vapor–solid system, described by the Lennard-Jones interaction potential, and found the growth for average radii of the first and second layers to be in the form $R^2(t) = C\log(t) + D$ with $C \approx 430$ and 272 for the first and second layers, respectively. This relation disagreed with the $R^2(t) \sim t$ reported in experimental studies using nonvolatile liquids (Heslot *et al* 1989, Cazabat *et al* 1990), and the discrepancy was attributed to vapor condensation ahead of the drop and the small number of molecules used in the simulation. Kandlikar *et al* (2001) studied the spreading of a liquid water droplet in contact with a platinum surface and found that the spreading area is proportional to the one-third power of time. Other studies based on MD simulations (Jang *et al* 1992, Nieminen *et al* 1992) reported that the spreading was much slower than that observed experimentally, and close to $R^2(t) \approx \log(t)$, and the precursor film was spreading linearly in time.

As discussed above, the droplet spreading behavior on solid surfaces has been extensively investigated, and a good understanding of the phenomena has been achieved. However, there are many fundamental issues, which are not fully understood, especially at submicron and nanoscales. Most numerical studies have considered sessile drops in two-dimensional (2D) and cylindrical configurations, and many of them have focused on the dynamics of the precursor film. Moreover, there are noticeable discrepancies in the scaling relationships reported for the temporal variation of spread diameter and contact angle. The major objective of the present study is to examine the spontaneous spreading behavior of a nanodroplet on surfaces with different wetting characteristics. A numerical approach based on MD

Table 1. System properties used in MD simulations.

				$N_{\text{Particles}}$			
D_0 (nm)	ε_w	ε_f	Box dimension (σ)	Total	Drop	Surface	Ambient
6	1, 0.15, 0.05	1.0	$34.9 \times 34.9 \times 69.8$	5553	2123	2440	990
9	1, 0.15, 0.05	1.0	$52.4 \times 52.4 \times 104.8$	21232	7011	10920	3301
12	1, 0.15, 0.05	1.0	$69.8 \times 69.8 \times 139.7$	44048	16757	19360	7931

simulations is employed. This approach has been shown to be quite effective for investigating droplet processes at the nanoscale (Consolini *et al* 2003, Sedighi *et al* 2010). Simulation results are used to obtain scaling relationships for describing the temporal variation of dynamic contact angle and spreading diameter, and the effect of droplet size on the spreading characteristics. In this context, previous scaling laws based on hydrodynamic and molecular kinetic models are also examined for the spontaneous spreading of nanodroplets. The present study is also motivated by our previous investigation that focused on the forced spreading. Thus, the results of these two studies are used to compare the dynamics of spontaneous and forced spreading.

2. The physical–numerical model

The physical–numerical model and the various parameters used are the same as those used for the forced spreading discussed in our previous investigation (Sedighi *et al* 2010). An initially spherical droplet surrounded by ambient gas is located at the center of a solid surface. The liquid, solid and ambient gases are represented in this study by a Lennard-Jones potential. As there is no initial velocity imposed on the droplet, it is expected to spread under the effects of viscous and surface forces. The simulation system is a 3D box that consists of 44 048 argon atoms,[3] constituting the liquid droplet, solid surface and ambient gas atoms. The interactions between molecules are represented by the potential

$$\phi(r) = 4\varepsilon[(\sigma/r)^{12} - (\sigma/r)^{6}] \tag{1}$$

where σ and ε are the characteristic length and energy parameters of the Lennard-Jones (LJ) potential. For the droplet, molecules are modeled as argon atoms with $\sigma = 3.405$ Å and $\varepsilon = 1.67 \times 10^{-21}$ J. The parameters of the solid wall were varied to represent a range of surface wettability. The potential was truncated at a cut-off distance of 3σ, as is usual in such models (Allen and Tildesley 1987). The dimensions of the simulation box and the values of various parameters used in simulations are provided in table 1. The liquid density and temperature are $0.75\sigma^{-3}$ and $0.72\varepsilon/k$, respectively. The fluid particles can move freely in the 3D system and periodic boundary conditions are employed at the system boundaries. For the results shown, we used $\rho_w = 0.75\sigma^{-3}$ for the droplet. The surrounding (ambient) gas had an initial density of $\rho_a = 0.0167\rho_f$, and the reduced initial temperature was $T^* = kT/\varepsilon = 0.72$. Note that the subscripts f, a and w denote the droplet fluid, ambient fluid and wall (surface), respectively.

The surface–surface interactions were also modeled with the LJ potential. Each wall atom was attached to the lattice site with a simple harmonic potential, with a spring constant of $K = 100\varepsilon/\sigma^2$, and is allowed to oscillate due to thermal fluctuations around its lattice position. The equations of motion were integrated using Gear's fifth-order predictor–corrector

[3] This value corresponds to the 12 nm droplet case.

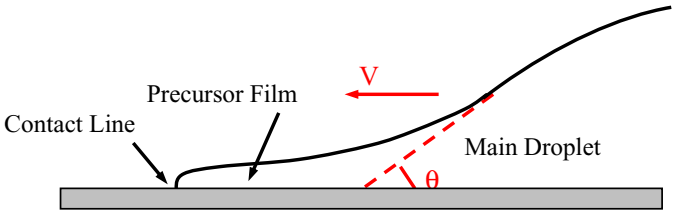

Figure 1. Schematic diagram of the spontaneous spreading of a liquid droplet on a solid surface, showing the spreading of a precursor film in front of the droplet. Here θ is the dynamic contact angle and V the velocity of the contact line.

algorithm. The time step is $\Delta t = 0.005\tau = 1.078 \times 10^{-2}$ ps, where $\tau = (m\sigma^2/\varepsilon)^{1/2}$ with m being the mass of the argon atom. Unless noted otherwise, all variables are normalized with respect to argon parameters ($\varepsilon = 1.67 \times 10^{-21}$ J, $\sigma = 3.405$ Å and $m = 39.948$ amu). Thus, the characteristic length and time scales for normalizing are $\sigma = 3.405$ Å and $t_0 = \tau = 2.156 \times 10^{-12}$ s. The initial droplet configuration was stabilized for approximately 500 time steps before the dynamics of the spreading were examined. The coordinates of all molecules were sampled every 500 steps for subsequent analysis. To investigate the dynamics of droplet spreading and contact angle evolution, an algorithm was developed to track the interface and compute the contact angle using density profiles. The liquid–vapor interface was defined when the density is approximately 25% of the bulk liquid value. This interface was then used to compute contact angle (slope of the curve passing through the interfacial points). The uncertainty in the calculation of contact angle is generally less than 10%. The spreading diameter and time evolution of spreading were monitored at different stages of the spreading process. Further details are provided in Sedighi (2010) and Sedighi *et al* (2010).

3. Results and discussion

We now present the results of MD simulations dealing with the spontaneous spreading of a droplet on flat surfaces with different wetting characteristics. First, we discuss the dynamics of a precursor film, which characterizes the early stage of spontaneous spreading, followed by the discussion of global spreading characteristics. The results then focus on a comparison of spontaneous spreading with forced spreading. Finally, the correlations are presented to characterize the effect of droplet size on the dynamic contact angle, spread diameter and contact line velocity.

3.1. Dynamics of a precursor film

As discussed by de Gennes (1985), the driving force for the spontaneous spreading of a liquid droplet is given by a spreading coefficient defined as

$$S = \gamma_{\mathrm{lv}}(\cos\theta - 1). \tag{2}$$

Here γ_{lv} is the liquid-vapor free surface energy and θ the contact angle. As discussed in Bascom *et al* (1964) and de Gennes (1985), the necessary condition for the spreading coefficient to be positive is that the contact angle be zero, implying that spontaneous spreading occurs through a precursor film developing in front of the droplet. This is shown schematically in figure 1, with a precursor film spreading to the left ahead of the droplet. The dynamics of spontaneous spreading during the early stage are characterized by this precursor film.

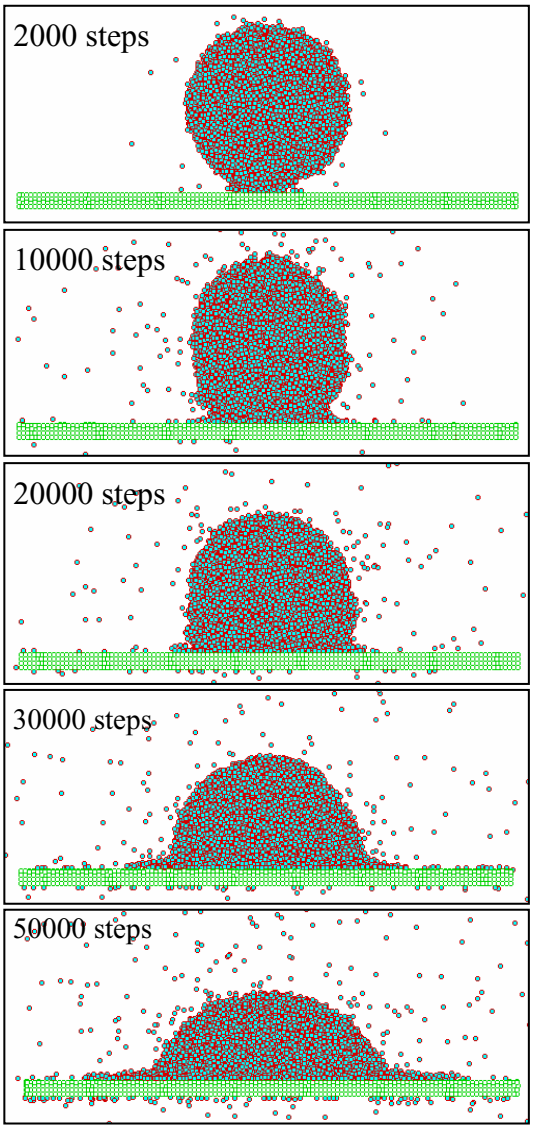

Figure 2. Snapshots or computed images showing the dynamics of spreading during the early stage of spontaneous spreading of a 12 nm droplet on a wettable surface with $\varepsilon_w = 1$. Images depict the development and spreading of the precursor film in front of the droplet.

Figure 2 presents the computed images for a 12 nm droplet during the early stage of spreading on a wettable surface. These images clearly depict the development and motion of the precursor film. The precursor foot can be easily distinguished from the main droplet in snapshots at 30 000 and 50 000 time steps (~ 0.32 and 0.54 ns). At later times, as the film base diameter increases, its advancing front becomes thinner. The liquid atoms in this part gradually lose their close connection with each other, and form scattered clusters around the droplet, which later turn into individual atoms and evaporate from the surface. As a consequence, tracking of the precursor film becomes difficult, and its diameter cannot be determined accurately. In addition, the thick part of the film joins with the main droplet and

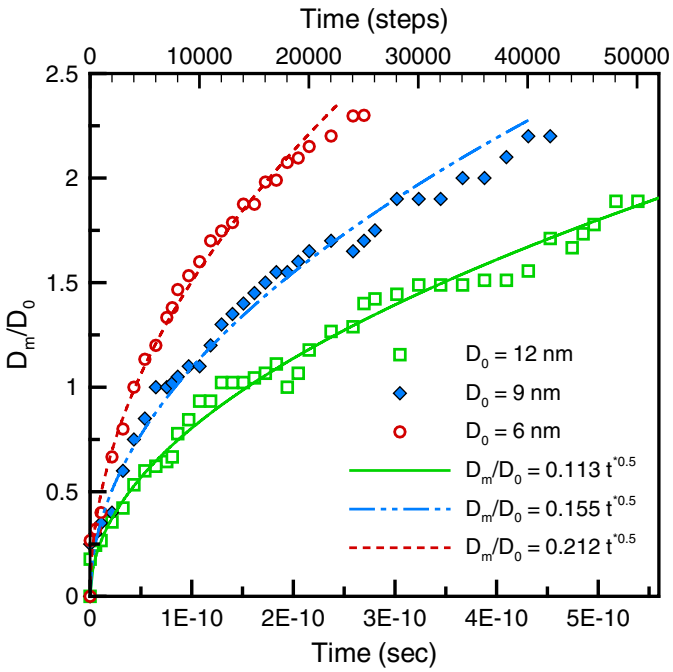

Figure 3. Temporal variation of the precursor film diameter for the spontaneous spreading of three different-sized droplets on a wettable surface with $\varepsilon_w = 1.0$. Correlations for the variation of the normalized diameter with normalized time obtained from a regression analysis are also indicated.

spreads at the same speed as the droplet. Figure 3 presents the temporal variation of precursor film diameter, normalized by the initial droplet diameter, for three different-sized droplets spreading on a wettable surface. The regression analysis of the data for the three droplets yielded the following correlation for the temporal variation of the normalized film diameter, $d = D_m/D_0 \propto t^{0.5\pm0.03}$, which is in good agreement with the reported experimental data (Voue and De Coninck 2000), indicating the diffusive nature of the spreading process.

3.2. Scaling of spreading diameter and contact angle with time

The dynamic characteristics of spontaneous spreading on a wettable surface are depicted in figure 4, which plots the spreading diameter and contact angle versus time for three different-sized droplets. The corresponding results for a non-wettable surface are shown in figure 5.[4] Note that the spreading behavior depicted in figure 4 for the wettable surface is qualitatively consistent with that reported in previous studies (Schiaffino and Sonin 1997, de Ruijter *et al* 1999a, 1999b, Forester *et al* 2001, Roux and Cooper-White 2004). However, the effect of droplet size on spreading dynamics was not examined in these studies. This aspect is further discussed in sections 3.4 and 3.5.

For all three surfaces, as time increases, the spreading diameter increases while the contact angle decreases monotonically towards its equilibrium value. However, there are important differences, which can be attributed to surface wettability. As the wettability decreases, the spreading process becomes increasingly slower. As indicated in figures 4 and 5,

[4] Results for a partially wettable surface (with $\varepsilon_w = 0.15$) were qualitatively similar to those for the non-wettable surface in figure 5, and are further discussed in Tanner (1979).

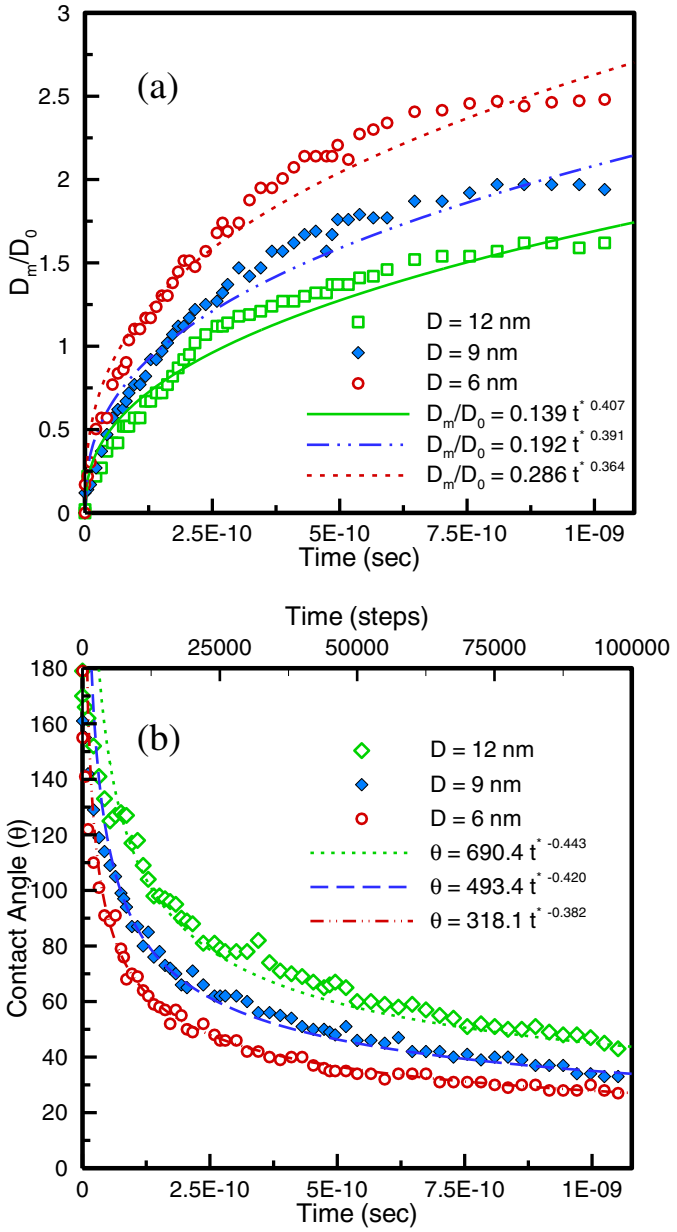

Figure 4. Temporal evolution of normalized (a) dynamic contact angle and (b) spreading diameter for three different-sized droplets spreading spontaneously on a wettable surface with $\varepsilon_w = 1.0$. Time is given in seconds as well as in number of time steps, with step size of $\Delta t = 1.078 \times 10^{-14}$ s.

the temporal rates of change of spreading diameter and contact angle decrease as the surface wettability is reduced. A regression analysis was used to obtain correlations for the temporal variation of spreading diameter and contact angle for surfaces with different wettability. These correlations for the three surfaces are listed in table 2 and also included in respective figures. The table also lists the commonly used scaling laws based on the hydrodynamic theory (i.e. Tanner's law) (Voinov 1976, Tanner 1979) and molecular kinetic theory (Blake and

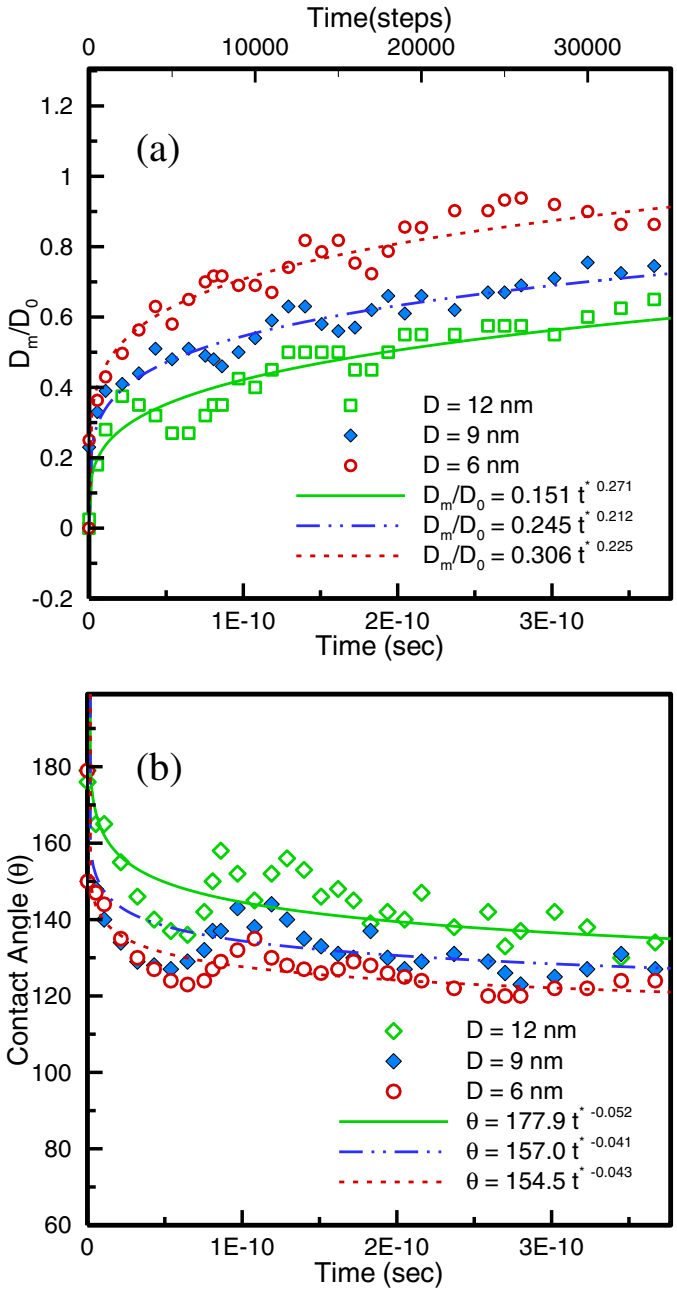

Figure 5. Temporal evolution of normalized spreading diameter (a) and contact angle (b) for three different-sized droplets spreading spontaneously on a non-wettable surface with $\varepsilon_w = 0.05$. Time is given in seconds as well as in number of time steps, with step size of $\Delta t = 1.078 \times 10^{-14}$ s.

Haynes 1969, Cherry and Holmes 1969). In previous studies, these scaling laws have been generally discussed in the context of wettable and partially wettable surfaces. Note that the spreading process on a wettable surface can be described by three different stages, namely the initial, intermediate and final stages. These three stages are characterized by different

Table 2. Correlations for the variation of the normalized spreading diameter and contact angle for spontaneous spreading on wettable, partially wettable and non-wettable surfaces.

Cases	Spreading diameter	Contact angle
Hydrodynamics theory	$d \sim t^{1/10}$	$\theta \sim t^{-3/10}$
Molecular kinetic theory	$d \sim t^{1/7}$	$\theta \sim t^{-3/7}$
Simulations: wettable surface	$d \sim t^{0.54\pm0.03}$ Initial stage	
	$d \sim t^{0.2\pm0.04}$ Intermediate stage	$\theta \sim t^{-0.42\pm0.02}$
	$d \sim t^{0.16\pm0.04}$ Final stage	
Simulations: partially wettable	$d \sim t^{0.25\pm0.03}$	$\theta \sim t^{-0.07\pm0.03}$
Simulations: non-wettable	$d \sim t^{0.23\pm0.04}$	$\theta \sim t^{-0.044\pm0.007}$

Note that the correlations obtained from simulations are for 12, 9 and 6 nm diameter droplets. Some deviations for the 6 nm diameter droplets are noted in the text. Here $d = D_m/D_0$, θ is in degrees and t is in seconds.

rates of spreading, as shown in figures 6(a)–(c), respectively. The curve fit or correlations obtained using regression analysis for each stage are also indicated in these figures and table 2. It is interesting to note that the scaling of spread diameter during the initial stage is nearly the same as that for the precursor base diameter, implying that the initial spreading stage is mainly determined by the dynamics of the precursor film.

Results for the intermediate stage yield the following correlations for the normalized spreading diameter versus time: $d \sim t^{0.2\pm0.04}$ for all three droplet sizes. The corresponding correlation for the dynamic contact angle, which applies to all three stages, is given by $\theta \sim t^{-0.42\pm0.02}$ (cf table 2 and figure 4). Comparing these scaling equations with the classical scaling laws, which have been extensively discussed in the literature, indicates that the present simulations yield correlations that are relatively closer to those based on the molecular kinetic model. Our scaling equations are also consistent with those reported in previous numerical and experimental studies. For instance, Yaneva *et al* (2003) reported the spreading diameter scaling as $d \sim t^{0.24}$, whereas the experimental studies of Poulard and Cazabat (2005) Poulard *et al* (2006) reported the following correlations: $d \sim t^{0.20}$ and $d \sim t^{0.19}$, respectively. Results for the third spreading stage, plotted in figure 6(c), yield the following correlations: $d \sim t^{0.18\pm0.05}$, $d \sim t^{0.14\pm0.02}$ and $d \sim t^{0.12\pm0.014}$ for 12, 9 and 6 nm droplets, respectively. These correlations also exhibit relatively good agreement with those based on the molecular kinetic model.

Results for the temporal variation of the spreading diameter and contact angle for the non-wettable surface are presented in figure 5. The regression analysis of these data yielded the following correlations: $d \sim t^{0.25\pm0.03}$ and $\theta \sim t^{-0.07\pm0.03}$ for the partially wettable surface (with $\varepsilon_w = 0.15$) and $d \sim t^{0.23\pm0.04}$ and $\theta \sim t^{-0.044\pm0.007}$ for the non-wettable surface. The results for the non-wettable surface may not be compared to the hydrodynamic or molecular kinetic model because these models have generally been discussed in the context of wettable and partially wettable surfaces. Another notable feature from figure 5 pertains to the oscillations associated with spontaneous spreading on a non-wettable surface. These oscillations are more easily discernible in the dynamic contact angle plots in these figures. In addition, as surface wettability decreases, the amplitude of oscillations seems to increase.

3.3. Spontaneous spreading versus forced spreading

In a previous study, we examined the dynamics of forced spreading on surfaces with different wetting characteristics (Sedighi *et al* 2010). Therefore, it is relevant here to compare the

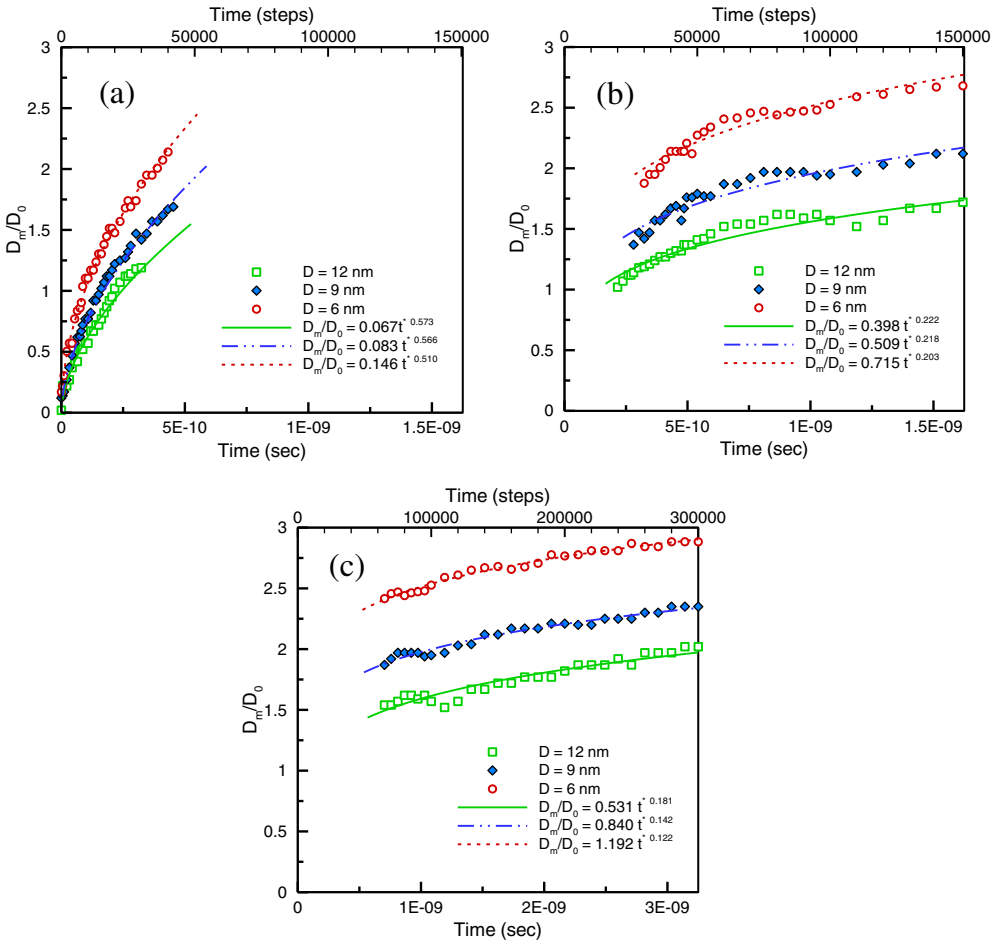

Figure 6. Temporal evolution of the normalized spreading diameter for three different-sized droplets spreading on a wettable surface with $\varepsilon_w = 1.0$: the initial (a), intermediate (b) and final (c) stages of spreading.

spreading behavior under the forced and spontaneous conditions. Figure 7 presents images from simulations at various times for the spontaneous spreading of a 12 nm droplet on wettable ($\varepsilon = 1$), partially wettable ($\varepsilon = 0.15$) and non-wettable ($\varepsilon = 0.05$) surfaces. The corresponding images for the forced spreading are depicted in figure 8. Numerical results in terms of the temporal variation of spread diameter and contact angle for the forced and spontaneous cases are presented in figures 9–11. In the following, we highlight the differences between the spontaneous spreading and forced spreading on different surfaces.

The major differences between the spontaneous and forced spreading on a wettable surface are due to the presence of a precursor film and significantly lower spreading rate in the case of spontaneous spreading (cf figures 7–9). The precursor film can be observed in images at 30 000, 50 000 and 80 000 time steps in figure 7. Thus, for the spontaneous spreading case, the initial spreading process is characterized by the development of a precursor film, which moves ahead of the droplet. On the other hand, for the forced spreading, the initial spreading process is characterized by a rapid increase in spread diameter, along with a rapid decrease

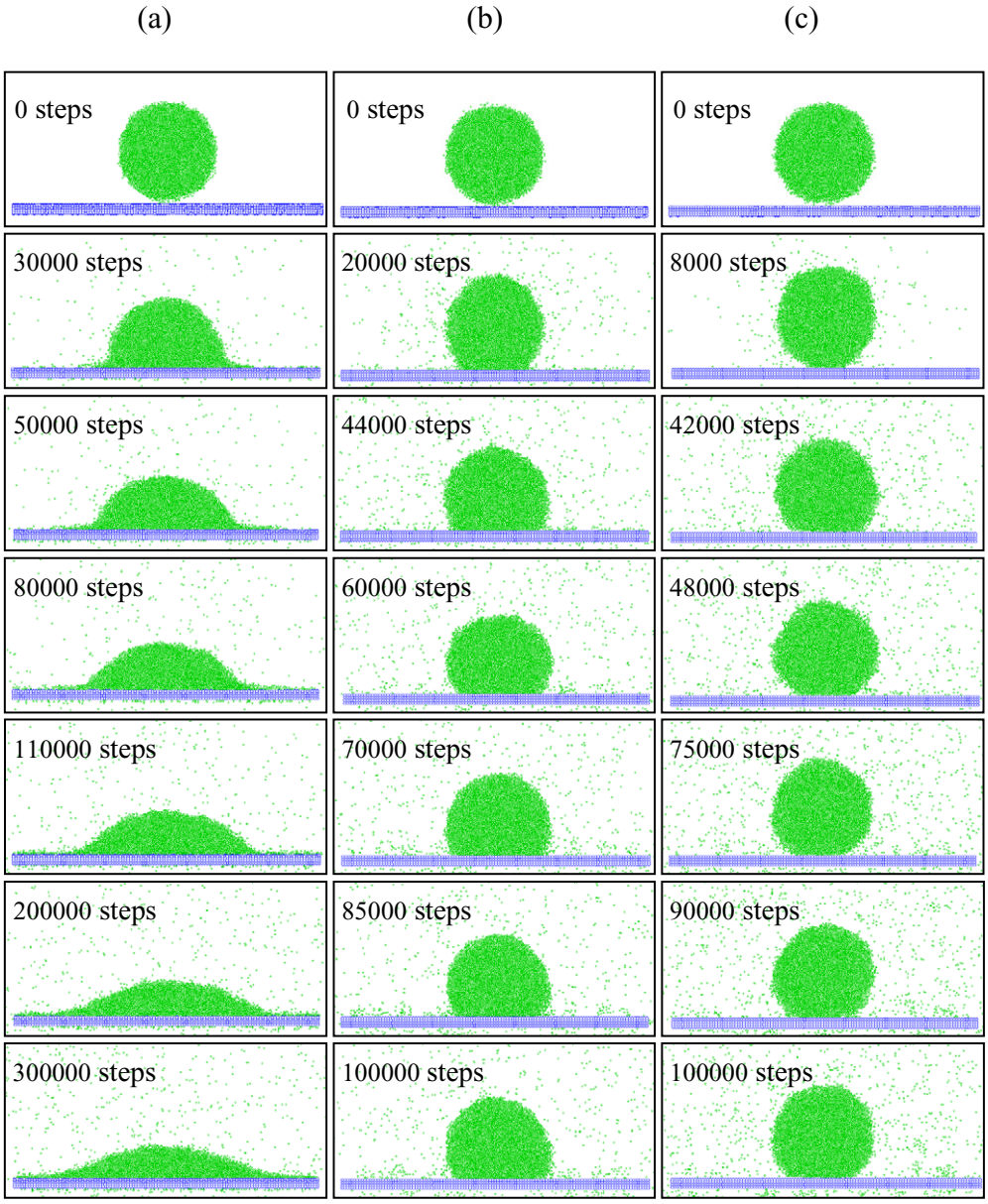

Figure 7. Images showing the dynamics of spontaneous spreading (with initial velocity $V_0 = 0$) of 12 nm droplets on three flat surfaces with different wetting characteristics: (a) wettable, $\varepsilon_w = 1.0$, (b) partially wettable, $\varepsilon_w = 0.15$, and (c) non-wettable, $\varepsilon_w = 0.05$.

in contact angle. This is due to the initially high initial kinetic energy of the droplet. The difference in the spreading rates, especially during the early stage, can be easily discerned in figure 9, which plots the temporal evolution of spreading diameter and contact angle for the two cases. The rate of increase of spreading diameter (or contact line velocity) for forced spreading is about three times higher than that for spontaneous spreading. At later times, the spreading rates slow down for both spontaneous and forced spreading, and the contact angle

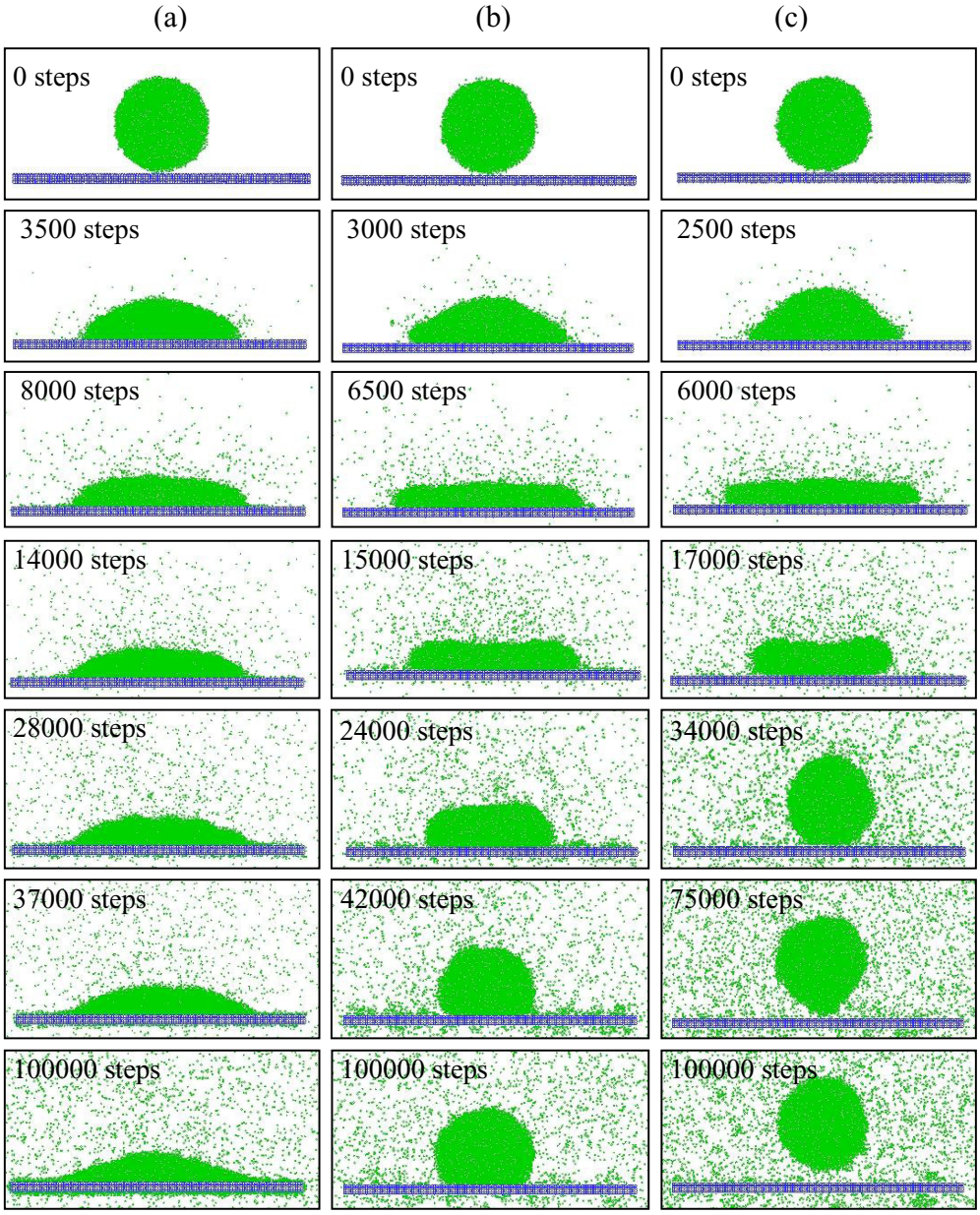

Figure 8. Images showing the dynamics of forced spreading of 12 nm droplets with initial velocity $V_0 = 1.25\,\mathrm{m\,s^{-1}}$ on three flat surfaces with different wetting characteristics: (a) wettable, $\varepsilon_w = 1.0$, (b) partially wettable, $\varepsilon_w = 0.15$, and (c) non-wettable, $\varepsilon_w = 0.05$.

approaches its equilibrium value. It is also interesting to note that while the spreading rates are different, the equilibrium contact angles for the two cases are nearly the same.

There are other fundamental differences between spontaneous and forced spreading for partially wettable and non-wettable surfaces. In particular, the spreading process in the case of forced spreading is characterized by advancing and receding stages, as indicated by the computed images in figure 8 and the plots of spread diameter and contact angle in figures 10

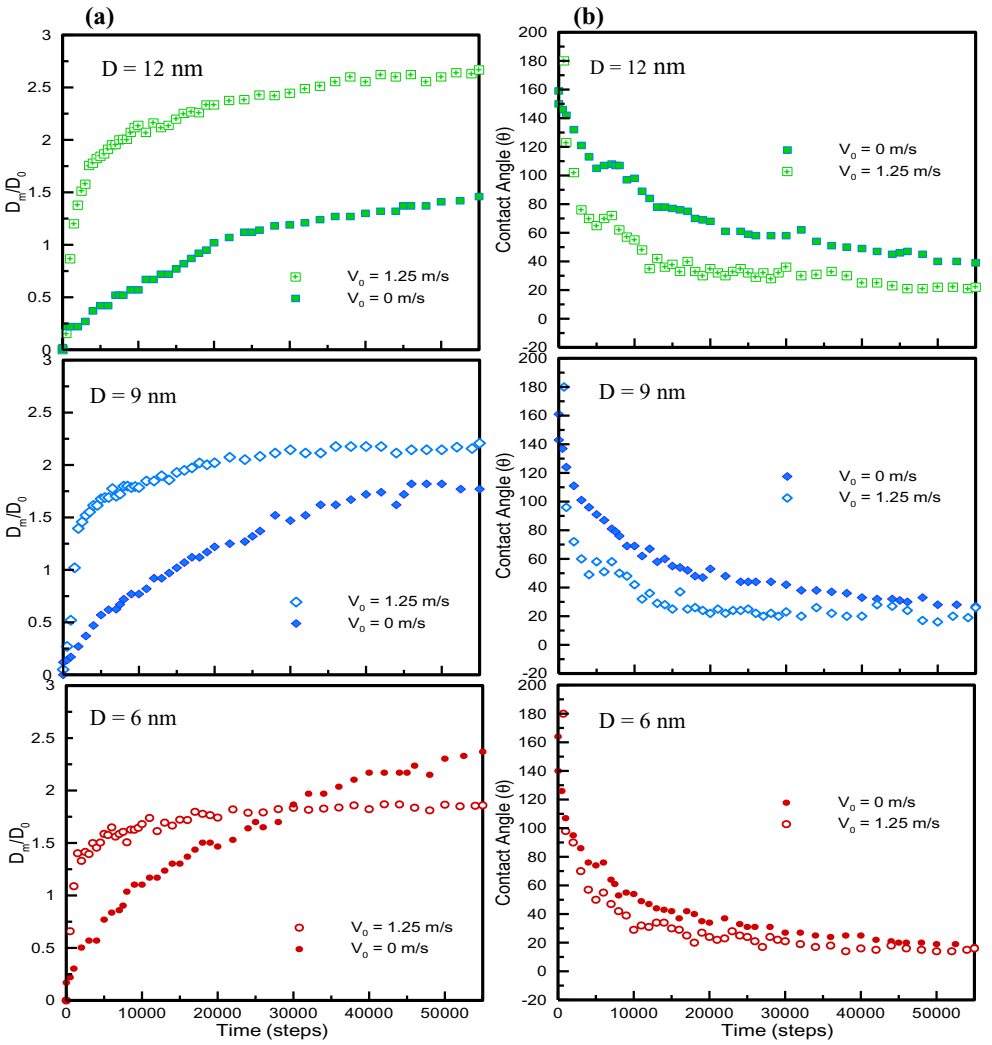

Figure 9. Comparison of spontaneous ($V_0 = 0$) and forced spreading ($V_0 = 1.25\,\mathrm{m\,s^{-1}}$) in terms of the temporal variation of (a) the spreading diameter and (b) dynamic contact angle for three different-sized droplets spreading on wettable surface with $\varepsilon_w = 1$. Time is given in terms of the number of time steps, with step size of $\Delta t = 1.078 \times 10^{-14}$ s.

and 11. In addition, as indicated in figure 11, the spreading process involves droplet bounce-off from a non-wettable surface. The bounce-off can be observed in images at 75 000 and 100 000 time steps in figure 8, as well as in figure 11. In contrast, for the spontaneous spreading, the droplet spreads slowly to its equilibrium configuration for both partially wettable and non-wettable surfaces. In addition, as noted earlier, as the droplet spreads it undergoes oscillations, which are more clearly visible in the contact angle plots in figures 10 and 11 for the spontaneous spreading case. Finally, it is interesting to note that while the dynamic spreading processes are markedly different, the equilibrium contact angles are nearly the same for the forced and spontaneous spreading cases.

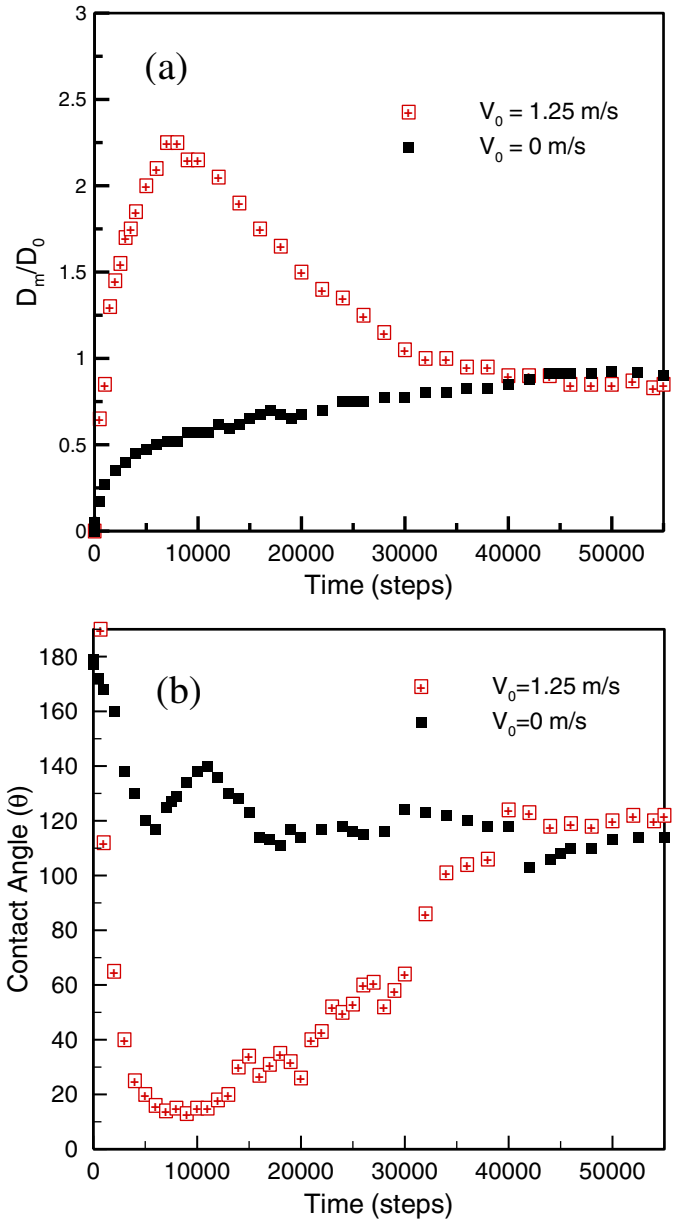

Figure 10. Comparison of spontaneous ($V_0 = 0$) and forced spreading ($V_0 = 1.25\,\mathrm{m\,s^{-1}}$) in terms of the temporal variation of (a) the spreading diameter and (b) dynamic contact angle for a 12 nm droplet spreading on a partially wettable surface with $\varepsilon_w = 0.15$. Time is given in terms of the number of time steps, with $\Delta t = 1.078 \times 10^{-14}$ s.

3.4. Effect of droplet size on the dynamics of spontaneous spreading

Another significant difference between spontaneous and forced spreading is due to the effect of droplet size on the spreading behavior. Results for spontaneous spreading are presented in figures 4 and 5 in terms of the temporal evolution of the normalized spreading diameter and

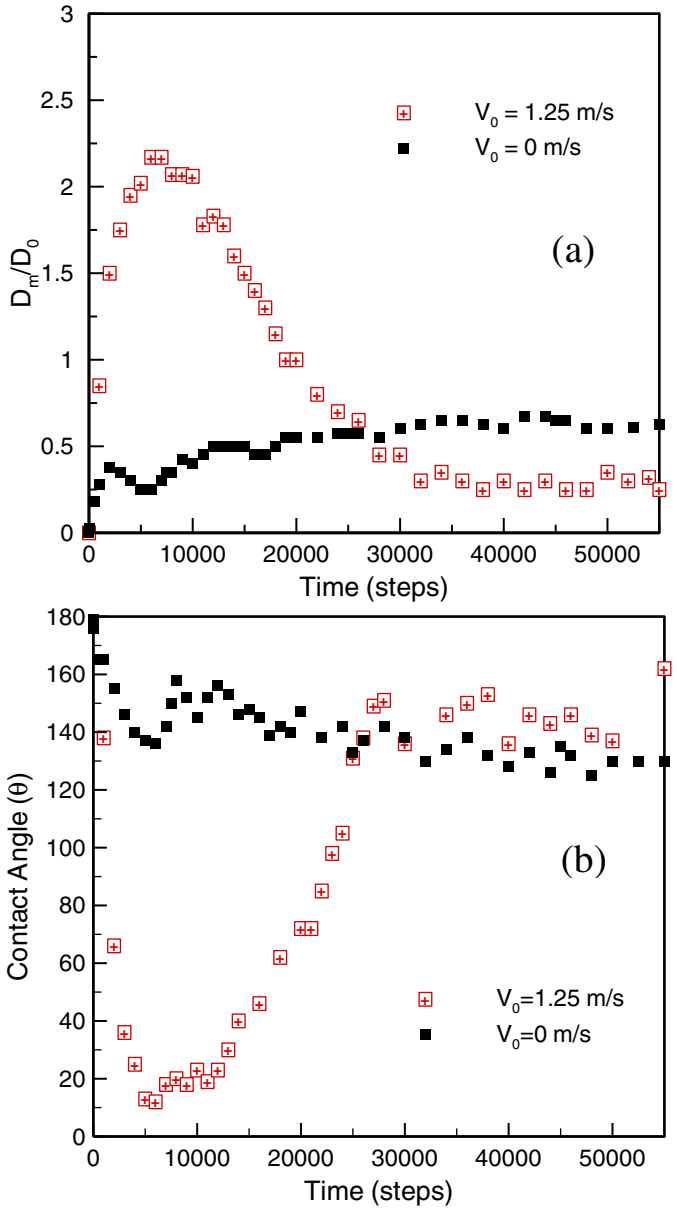

Figure 11. Comparison of spontaneous ($V_0 = 0$) and forced spreading ($V_0 = 1.25\,\mathrm{m\,s^{-1}}$) in terms of the temporal variation of (a) the spreading diameter and (b) dynamic contact angle for a 12 nm droplet spreading on a non-wettable surface with $\varepsilon_w = 0.05$. Time is given in terms of the number of time steps, with $\Delta t = 1.078 \times 10^{-14}$ s.

contact angle for different-sized droplets spreading on different surfaces. The corresponding results for forced spreading are shown in figures 5–7 of Sedighi *et al* (2010). An important observation from figures 4 and 5 is that for spontaneous spreading, as the droplet size increases, the spreading process becomes slower; that is, the increase in spread diameter and the decrease in contact angle occur at lower rates. Thus, at a given instant of time, the spread

diameter is smaller and the contact angle is larger for the larger droplet case. For instance, for the wettable surface, the normalized spread diameter values at equilibrium are 2.6, 1.9 and 1.5 for the 6, 9 and 12 nm droplets, respectively. The corresponding equilibrium contact angles for the three droplets are 15°, 18° and 20°, respectively. On the other hand, for the forced spreading case, the effect of droplet size has an opposite effect on the spreading rate (cf figure 5 in Sedighi *et al* (2010)); that is, as the droplet size is increased, a larger droplet spreads faster than a smaller droplet. Consequently, the normalized spread diameter values at equilibrium for the forced spreading case are 1.75, 2.1 and 2.6 for 6, 9 and 12 nm droplets, respectively. The results for partially wettable and non-wettable surfaces also exhibit this opposite trend with respect to the effect of droplet size on the spontaneous and forced spreading. However, for these surfaces, aspects pertaining to the advancing and receding stages and the droplet bounce-off become more important, as discussed in the preceding section.

3.5. Scaling relationships for the effect of droplet size

In our previous study dealing with forced spreading (Sedighi *et al* 2010), scaling relationships were developed to describe the effect of droplet size on the spreading characteristics. Here, we develop similar relationships for the spontaneous spreading. By following a similar procedure to that used in the previous study, the following relations are obtained for the effect of droplet size on the spreading diameter, contact angle and spreading time:

$$D_m/D_0 \propto (D_0/\sigma)^{-0.6\pm0.04}, \tag{3}$$

$$\theta_{\mathrm{R}} \propto (D_0/\sigma)^{0.67\pm0.12}, \tag{4}$$

$$t/t_0 \propto (D_0/\sigma)^{0.25\pm0.05}. \tag{5}$$

Here D_m is the spread diameter, D_0 the initial droplet diameter and θ_{R} the rescaled contact angle, obtained by subtracting the equilibrium contact angle from its instantaneous value. The above correlations are valid for spontaneous spreading on all three surfaces investigated. Following a similar procedure and using the data presented in figure 3, the following relationships were obtained for the scaling of precursor film diameter and spreading time with the droplet size:

$$D_m/D_0 \propto (D_0/\sigma)^{-0.5\pm0.02}, \tag{6}$$

$$t/t_0 \propto (D_0/\sigma)^{0.5\pm0.03}. \tag{7}$$

Figures 12 and 13 present the rescaled contact angle and spreading diameter (based on equations (3) and (4) plotted versus the rescaled time (equation (5)) for the wettable and non-wettable surfaces, respectively. As mentioned earlier, the results for the partially wettable case are qualitatively similar to those for the non-wettable case, and are not shown here but can be seen in Sedighi (2010). Similarly, figure 14 plots the rescaled spreading diameter for the precursor film (equation (6)) versus the rescaled time (equation (7)). These plots clearly demonstrate the validity of the above correlations, except for oscillations in the contact angle for partially wettable and non-wettable surfaces, as noted earlier. For comparison these rescaled plots should be compared with figures 4 and 5 on a one-to-one basis.

Finally, an attempt has been made to provide a physical basis for the above scaling relationships. Assuming that the inertia force plays a negligible role in the dynamics of spontaneous spreading, the spreading process may be described by the balance of surface and viscous forces, i.e. the viscous effects dissipate the driving energy of the surface force.

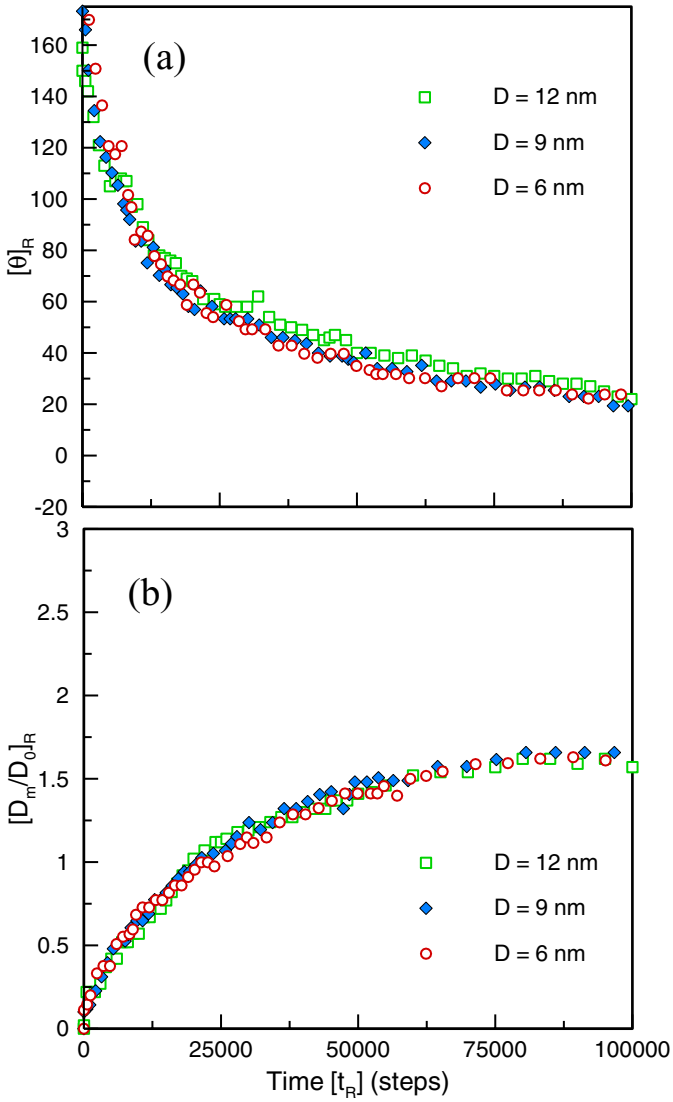

Figure 12. Rescaled (a) dynamic contact angle and (b) spreading diameter plotted versus rescaled time for three different-sized droplets spreading on a wettable surface with $\varepsilon_w = 1.0$.

Then the ratio of viscous dissipative energy and surface energy can be written as

$$R_1 = \frac{\mu(V_{CL}/h)D_m^3}{\gamma D_m^2}, \tag{8}$$

where γ, μ, V_{CL} and h are the surface tension, viscosity, velocity of the contact line and thickness of the liquid layer during spreading, respectively. Using $D_0^3 \propto hD_m^2$, based on the conservation of droplet volume during the spreading process, equation (8) can be written as

$$R_1 = \frac{\mu V_{CL}}{\gamma} \cdot \frac{D_m^3}{D_0^3}. \tag{9}$$

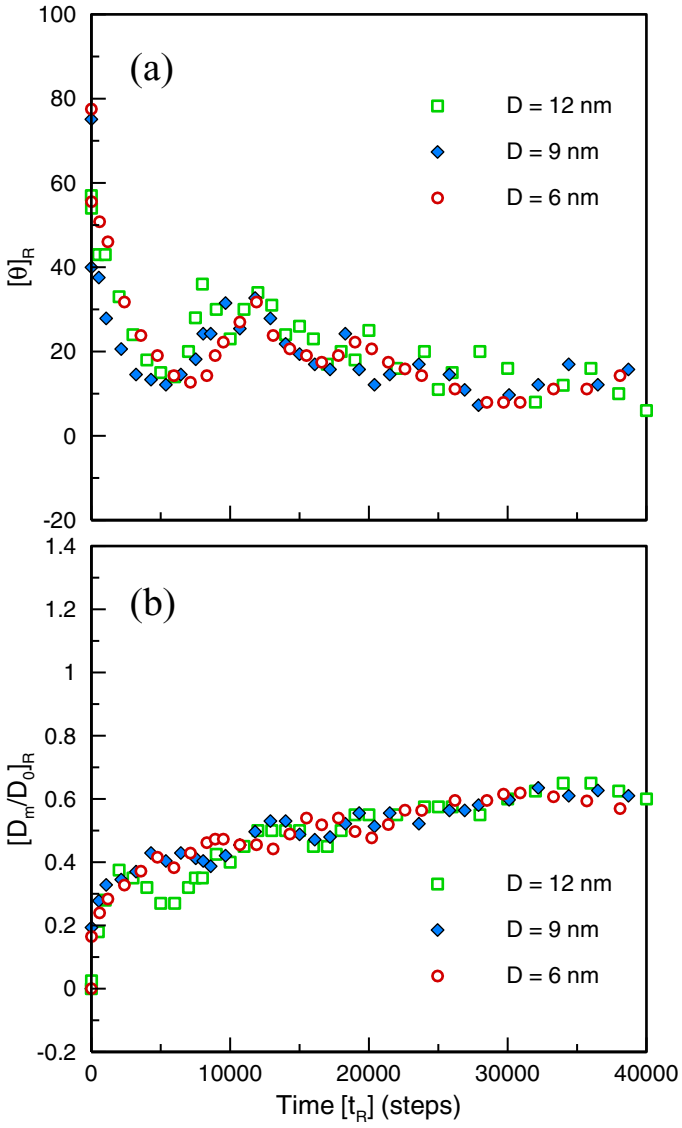

Figure 13. Rescaled (a) dynamic contact angle and (b) spreading diameter plotted versus rescaled time for three different-sized droplets spreading on a non-wettable surface with $\varepsilon_w = 0.05$.

Here $Ca = \mu V_{CL}/\gamma$ is the capillary number. For a given fluid and surface, equation (10) can be rewritten as

$$\frac{D_{m1}/D_{01}}{D_{m2}/D_{02}} = \left(\frac{V_{CL1}}{V_{CL2}}\right)^{-1/3}. \tag{10}$$

To obtain the scaling of spread diameter with respect to the droplet size, a scaling relationship is required between the contact line velocity (V_{CL}) and the droplet size. Blake and Haynes (1969) reported the dependence of contact line velocity on the contact angle as $\theta^3 \propto V_{CL}$. However, its scaling with respect to droplet size has not been examined in

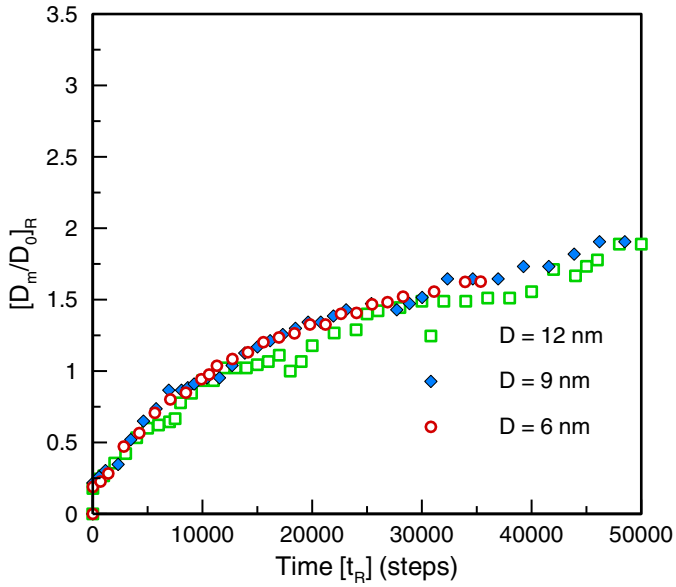

Figure 14. Rescaled spreading diameter of precursor film plotted versus rescaled time for three different-sized droplets spreading on a wettable surface with $\varepsilon_w = 1.0$.

previous studies. Consequently, we used simulation results to obtain such a correlation. Details are provided in Sedighi (2010). Essentially, V_{CL} was obtained from the computed variation of spread diameter with time, and then a regression analysis was used, yielding the following scaling relationship: $V_{CL}/V_{CL0} \propto (D_0/\sigma)^{1.69\pm0.52}$, with $V_{CL0} = \sigma/t_0$. Using this result in equation (10) yields

$$D_m/D_0 \propto (D_0/\sigma)^{-0.564}. \tag{11}$$

This is in good agreement with the scaling relationship, equation (3), obtained from our simulations.

4. Conclusions

MD simulations have been performed to investigate the spontaneous spreading behavior of nano-size droplets on flat surfaces with different wetting characteristics. The present study complements our previous investigation (Sedighi *et al* 2010) dealing with the forced spreading of a droplet on flat surfaces. Some important observations are given below.

The spontaneous spreading process on a wettable surface can be described in terms of three stages, namely the initial, intermediate and final stages. The initial stage is characterized by the development of a precursor film, which moves ahead of the droplet. The dynamics of this film have been analyzed in terms of the temporal variation of the film base diameter for 12, 9 and 6 nm diameter droplets. The regression analysis of the computed results for the three droplets yielded the following correlation for the temporal variation of the normalized film diameter, $d = D_m/D_0 \propto t^{0.5\pm0.03}$, which is in good agreement with the reported experimental data. A similar analysis of intermediate and final spreading stages, which occupy the bulk of the spreading period, yielded the following correlations for the spread diameter and contact angle: $d \sim t^{0.2\pm0.04}$ and $\theta \sim t^{-0.42\pm0.02}$, which are found to be in closer agreement with the

scaling laws based on the molecular kinetic model than with those based on the hydrodynamic model.

The dependence of contact angle, spreading diameter and the associated time period on the droplet size was analyzed and the following correlations were developed: $D_m/D_0 \propto (D_0/\sigma)^{-0.6}$, $\theta_R \propto (D_0/\sigma)^{2/3}$ and $t/t_0 \propto (D_0/\sigma)^{0.25}$, respectively. Global energy considerations are used to provide a physical basis for these correlations.

Significant differences are observed between the dynamics of spontaneous and forced spreading. These include the presence of a precursor film and slower spreading rates in the case of spontaneous spreading. In addition, the forced spreading involved advancing and receding stages on a partially wettable surface, and droplet bounce-off from a non-wettable surface. These phenomena were not observed in spontaneous spreading. Another fundamental difference is due to the effect of droplet size on the spreading process. For spontaneous spreading, the variation of spread diameter with droplet size is found to be $D_m/D_0 \propto D_0^{-0.6\pm0.04}$, whereas for forced spreading it is $D_m/D_0 \propto D_0^{0.5}$. Thus, a larger droplet spreads less than a smaller droplet in spontaneous spreading, whereas it spreads more in forced spreading.

Acknowledgments

This work was supported in part by a grant from the Office of Basic Energy Sciences, US Department of Energy (DE-FG02-86ER46538).

References

Allen M P and Tildesley D J 1987 *Computer Simulation of Liquids* (Oxford: Clarendon)

Bascom W D, Cottington R L and Singleterry C R 1964 *Contact Angle, Wettability and Adhesion* ed F M Fowkes (*Advances in Chemistry Series* 43) (Washington, DC: American Chemical Society) pp 355–79

Blake T D 1968 *PhD Thesis* University of Bristol

Blake T D 1993 *Wettability* ed J C Berg (New York: Marcel Dekker) pp 251–309

Blake T D and Haynes J M 1969 Kinetics of liquid/liquid displacements *J. Colloid Interface Sci.* **30** 421–3

Cazabat A M, Fraysse N and Heslot F 1990 *Prog. Colloid Polym. Sci.* **83** 52

Cherry B W and Holmes C M 1969 Kinetics of wetting of surfaces by polymers *J. Colloid Interface Sci.* **29** 174–6

Consolini L, Aggarwal S K and Murad S 2003 A molecular dynamics simulation of droplet evaporation *Int. J. Heat Mass Transfer* **46** 3179–88

Cox R G 1986 The dynamics of the spreading of liquids on a solid surface *J. Fluid Mech.* **168** 169–94

De Coninck J, De Ruijter M J and Voue M 2001 Dynamics of wetting *Curr. Opin. Colloid Interface Sci.* **6** 49–53

De Coninck J, Ortona U D, Koplik J and Banavar J 1995 *Phys. Rev. Lett.* **74** 928–31

de Gennes P G 1985 Wetting: statics and dynamics *Rev. Mod. Phys.* **57** 827–63

de Ruijter M, Blake T D, Clarke A and De Coninck J 1999a Droplet spreading: a tool to characterize surfaces at the microscopic scale *J. Petrol. Sci. Eng.* **24** 189–98

de Ruijter M J, De Coninck J and Oshanin G 1999b Droplet spreading: partial wetting regime revisited *Langmuir* **15** 2209–16

Decamps C and De Coninck J 2000 Dynamics of spontaneous spreading under electrowetting conditions *Langmuir* **16** 10150–3

Forester J E, Sunkel J M and Berg J C 2001 Spontaneous spreading of emulsions on solid surfaces: morphology and dynamics *J. Appl. Polym. Sci.* **81** 1817–25

Glasstone S, Laidler K J and Eyring H J 1941 *The Theory of Rate Processes* (New York: McGraw-Hill)

He G and Hadjiconstantinou N G 2003 A molecular view of Tanner's law: molecular dynamics simulations of droplet spreading *J. Fluid Mech.* **497** 123–32

Heine D R, Grest G S and Webb E B III 2003 *Phys. Rev.* E **68** 061603

Heine D R, Grest G S and Webb E B III 2004 *Phys. Rev.* E **70** 011606

Heslot F, Fraysse N and Cazabat A M 1989 Molecular layering in the spreading of wetting liquid drops *Nature* **338** 640–2

Jang J X, Koplick J and Banavar J 1992 *Phys. Rev.* A **46** 7738

Kandlikar S G, Maruyama S, Steinke M E and Kimura T 2001 Molecular dynamics simulation and measurement of contact angle of water droplet on a platinum surface *ASME Proc. Int. Mechanical Engineering Congress and Exposition (11–16 November 2001)* paper IMECE 01–2832

Lee J and Kim C J 2000 Surface-tension-driven microactuation based on continuous electro wetting *J. Microelectromech. Syst.* **9** 171–80

Leger L and Joanny J F 1992 *Rep. Prog. Phys.* **57** 431–86

Lopez J, Miller C A and Ruckenstein E 1976 Spreading kinetics of liquid drops on solids *J. Colloid Interface Sci.* **56** 460–8

Marmur A 1983 Equilibrium and spreading of liquids on solid surfaces *Adv. Colloid Interface Sci.* **19** 75–102

Nieminen J, Abraham D, Karttienen M and Kaski K 1992 *Phys. Rev. Lett.* **69** 124

Poulard C and Cazabat A M 2005 *Langmuir* **21** 6270–6

Poulard C, Voué M, De Coninck and Cazabat A M 2006 *Colloids Surfaces* A **282** 240–6

Roux D C D and Cooper-White J J 2004 Dynamics of water spreading on a glass surface *J. Colloid Interface Sci.* **277** 424–36

Ruckenstein E and Dunn C S 1977 *J. Colloid Interface Sci.* **59** 135

Schiaffino S and Sonin A A 1997 Molten droplet deposition and solidification at low Weber numbers *Phys. Fluids* **9** 3172–87

Sedighi N 2010 Investigation of spreading characteristics of nano-droplet on solid substrate using MD simulations *PhD Thesis* University of Illinois at Chicago

Sedighi N, Murad S and Aggarwal S K 2010 Molecular dynamics simulations of nanodroplet spreading on solid surfaces; effect of droplet size *Fluid Dyn. Res.* **42** 035501

Semal S, Voue M, de Ruijter M J, Dehuit J and De Coninck J 1999 Dynamics of spontaneous spreading on heterogeneous surfaces in a partial wetting regime *J. Phys. Chem.* B **103** 4854–61

Shikhmurzaev Y D 1997 Moving contact lines in liquid/liquid/solid systems *J. Fluid Mech.* **334** 211–49

Tanner L H 1979 Spreading of silicone oil drops on horizontal surfaces *J. Phys. D: Appl. Phys.* **12** 1473–84

Voinov O V 1976 Hydrodynamics of wetting *Fluid Dyn.* **11** 714–21

Voue M and De Coninck J 2000 Spreading and wetting at the microscopic scale: recent developments and perspectives *Acta Mater.* **48** 4405–17

Yaneva J, Milchev A and Binder K 2003 *Macromol. Theory Simul.* **12** 573–81

Yang J X, Koplik J and Banavar J R 1991 Molecular dynamics of drop spreading on a solid surface *Phys. Rev. Lett.* **67** 3539–42